Material fingerprinting as a potential tool to domain orebody hardness and enhancing the prediction of work index

J.R. van Duijvenbode[1], L.M. Cloete[2], M.S. Shishvan[1], and M.W.N. Buxton[1]

[1]Delft University of Technology, The Netherlands
[2]AngloGold Ashanti, South Africa

Geochemical and mineralogical datasets from Tropicana Gold Mine, Australia, have been used to define ore fingerprints. VNIR/SWIR spectral data were represented by four normalised wavelength regions and were clustered to form spectral classes. Sequentially, these spectral class proportions within a block and collocated XRF data were clustered to form material types (fingerprints). The material types were related to an Equotip-BWi correlation. These correlations can be used to extrapolate a hardness signature and generate a BWi proxy for different blocks. The combined fingerprints and BWi proxy can assist as a tool for enhancing the prediction of comminution behaviour. They can explain specific domain-related hardness variations. For example, one material type could be separated into a softer (~15-18 kWh/t), and harder (>20 kWh/t) material blend. This was accomplished using the commonly overlooked VNIR region at 605 nm. This outcome has significance for blending strategies.

INTRODUCTION

Understanding and domaining rock hardness within orebodies (e.g., crushability and grindability) is important for strategic and tactical geometallurgy; for example, for designing the comminution circuit and forecasting the throughput during the life of mine (Dominy *et al.*, 2018). The material hardness is one of the attributes which may have variable effects on the comminution circuit throughput. For example, material harder than expected may reduce the throughput or reduce recovery, because the feed is not sufficiently ground, and not all metal is liberated. However, material softer than expected may be processed with a higher throughput which may increase production rates.

Commonly, initial hardness modelling is undertaken based upon the mineralogical, metallurgical and comminution test results retrieved during feasibility studies (see for example King and Macdonald, 2016; Montoya *et al.*, 2011) or when a new mine expansion is planned (e.g., push back or new underground extraction area). However, these data often have a low number of samples and spatial resolution, and may be subject to error. Therefore, it would be beneficial if advantage can be taken of other datasets to improve the spatial resolution, and guide optimal sample selection for future test work. In certain commodities, this is done using samples taken during grade control (GC) drilling.

At the Tropicana Gold Mine in Australia, GC samples are routinely collected at one-metre intervals during reverse circulation drilling. Once collected, the samples are analysed in an on-site laboratory for geochemical and mineralogical composition. Geochemical data are collected using X-ray fluorescence (XRF) and mineralogical data using a spectrometer that uses the visible near-infrared (VNIR) and short-wave infrared (SWIR) portions of the electromagnetic spectrum. Conventional fire assaying techniques are used to determine the gold grade in a final prepared pulp. Historically, calibrated relationships have been applied to translate the obtained proxy measurements (XRF and VNIR/SWIR) into geometallurgical estimates (e.g., work index, or recovery) (Catto, 2015).

Unfortunately, these relationships are not tested and not sufficiently validated due to the amount of expensive metallurgical tests required. Wambeke *et al.*, (2018), have shown how the work index estimates at Tropicana can be improved on a local scale by the reconciliation of the predicted and measured ball mill performance. They also indicated that the work index is usually overestimated by these conversion relationships, but despite estimation bias, improving the estimates does lead to an improved characterisation of the future mill feed work index.

This paper demonstrates the construction of material fingerprints of larger mining blocks using the GC point data sources (point XRF and VNIR/SWIR measurements). In this context, a fingerprint is a material classification based on the similarity of the measured and constitutive material attributes (van Duijvenbode *et al.*, 2020). Ideally, these fingerprints are a better proxy for the constitutive hardness properties found within a small spatial area or domain (representing a material blend) compared to those of individual samples. This hypothesis will be confirmed by linking each fingerprint with the typical bond work index parameters characterising the milling behaviour of this material. It is found that specific material attributes may be proxies for the hardness and, therefore, could be estimated. Finally, it is shown how the learnt fingerprint (material type) work index relationships can be improved by further domaining the geochemical and mineralogical signatures within material classes.

GEOLOGY AND MINERALISATION

The Tropicana Gold Mine is situated in the Plumridge Terrane, a zone that separates the in situ eastern margin of the Yilgarn craton from the Albany-Fraser orogen, Western Australia (Figure 1a). The deposit was formed by fluid flow through a network of biotite-pyrite-bearing shear zones in the original granulite facies quartzofeldspathic gneisses. The mineralised zones are hosted within a sequence of high grade quartzofeldspathic and garnet-bearing gneisses, with amphibolites, granulites, metasedimentary cherts and pegmatites (Figure 1b). These mineralised zones occur as one or two laterally extensive planar lenses with a moderate dip. Within the mineralised zone, biotite, sericite and pyrite alteration replaced the metamorphic mafic minerals and feldspar (Blenkinsop and Doyle, 2014; Crawford and Doyle, 2016). Post mineralisation faulting resulted in four distinct structural domains, which are from north to south: Boston Shaker, Tropicana, Havana (including Havana Deeps) and Havana South.

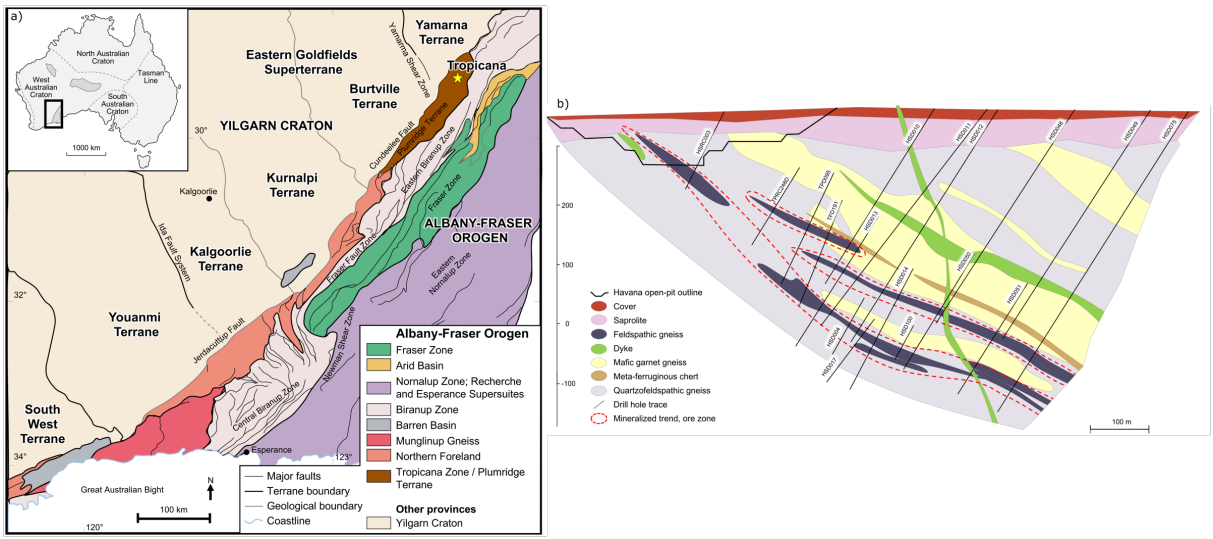

Figure 1. a) Geological map of the Albany-Fraser Orogen with respect to the eastern margin of the Yilgarn Craton, Western Australia, showing the location of the Tropicana gold deposit. Modified after Spaggiari et al., (2011). b) Schematic EW cross-section of the Havana South deposit (100 m thick at 649753 mE, 6761137 mN, azimuth 37°, GDA/UTM grid).

METHODS

Data were obtained from several sources from Tropicana Gold Mine (TGM). Most of the mineralogical (VNIR/SWIR) and geochemical data (XRF) are collected using the same samples from GC drilling. Spectral measurements were taken using an ASD TerraSpec mineral spectrometer (hereafter, referred to as TS data). Equotip rebound hardness measurements (unit is Leeb, Ls) were primarily taken on diamond drill core with intervals of one metre. The Bond Ball Mill Work Index (BWi in kWh/t) was infrequently taken on diamond drill cores. The variety of data obtained from measurements on different samples shows the difficulty of merging this data. To overcome this, all samples are assigned to blocks of a block model. These samples should relate to each other (material blend) and consequently, a block feature clustering approach can be applied. Figure 2a shows an exemplary spatial configuration of the different datasets found within an individual block and Figure 2b shows how the block data features translate into the block material fingerprint. The fingerprint is a combination of a separate TS data clustering approach described in the next sections and the XRF elemental concentrations. The initial assumption is that geochemistry and mineralogy largely explain the material hardness (Equotip, BWi).

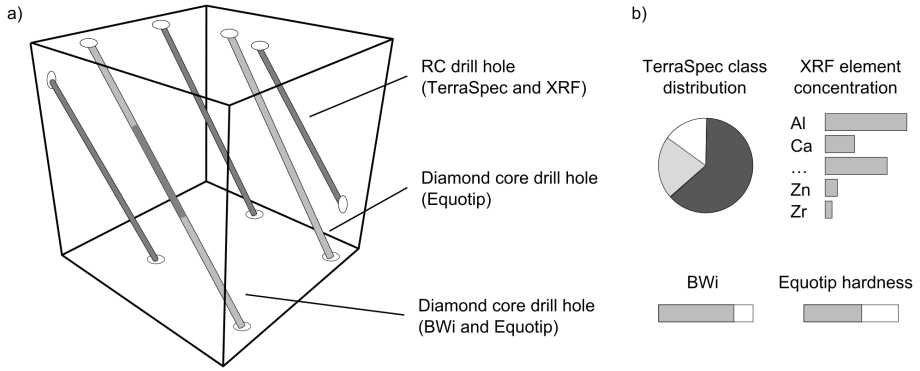

Figure 2. (a) Illustrative block of a block model with different drill holes indicating the different spatial locations where samples are taken; (b) the proportionality of TerraSpec classes and XRF elemental concentrations combined with the BWi and Equotip hardness determine the block features.

Mineralogical Data

The mineralogical dataset consists of about 142,000 (primarily) non-oxidised TS spectra with reflectance measurements of the VNIR and SWIR regions (500-2500 nm). The majority of these measurements are taken on drill chips from GC drilling and, therefore, have a dense spatial resolution. All analysis is done using raw unprocessed spectral responses, omitting the need for mineralogical identification (Ausspec, 2008). Additionally, it may reveal hitherto unrevealed textural or hardness signatures.

The individual spectra range from 350-2500 nm, and these were subdivided into four sub-regions for analysis. The selected regions and corresponding typical spectral response (Ausspec, 2008) are as follows:

- 500 – 750 nm: Fe-features, visible part of the spectra
- 1300 – 1450 nm: Water and OH features
- 1850 – 2000 nm: Water feature
- 2150 – 2400 nm: Al-OH (2180-2228), Fe-OH (2240-2298) and Mg-OH / CO_3 (2300-2370) mineral absorption features

The spectral response in each region was smoothed and normalised by a convex-hull removal (CHR) to remove dependence upon reflectance. This ensures that the spectra can be compared because the absorption features are only a function of depth and width (Ausspec, 2008). The benefit of this approach can be seen in the 500 – 750 nm region. Usually, these predominantly iron-related features are depressed due to the convex hull removal over the entire spectrum. However, doing this across a smaller region preserves features and increases their visibility. Figure 3a shows a typical TS spectrum with the four

regions of interest highlighted, and Figure 3b shows the normalised hull-quotient spectrum for each of the four regions.

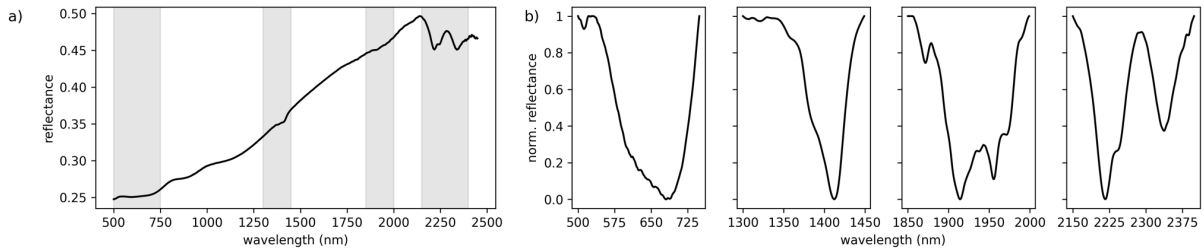

Figure 3. Convex-hull removal of TerraSpec spectrum; a) an example TerraSpec spectrum with the four selected regions used for clustering; b) normalised hull-quotient spectrum for each region.

The data from each region were combined, and each wavelength feature was normalised by removing the mean and scaling to unit variance. Then, the feature dimension was reduced by principal component analysis (PCA). The number of principal components (PCs) are automatically set to the amount which can describe 95% of the data variance. The lower-dimensional dataset functions as input for an agglomerative hierarchical clustering approach (Wierzchoń and Kłopotek, 2018). After clustering, each sample has a class label related to a specific suite of mineralogical signatures found within the three wavelength regions.

Geochemical Data

The geochemical dataset (142,000 samples) used in this study originates from portable XRF measurements taken from the same samples used for TS analysis. The concentrations of the following (15) elements are used in this study: Al, Ca, Cr, Fe, K, Mn, Nb, Pb, Rb, S, Si, Sr, Ti, Zn and Zr. The Au concentration is also known for these samples, but not further considered during clustering. Excluding Au from clustering ensures that emphasis is placed on major and other trace elements for classification (van Duijvenbode *et al.*, (*in press*).

Block Feature Clustering

Each individual sample has an assigned TS class obtained through TS clustering, and the set of elemental concentrations. The individual TS class characteristics are described; explanations of the elemental concentrations are only given where necessary (see van Duijvenbode *et al.*, (*in press*) for further detail). Subsequently, all block samples are merged together and further prepared for block feature clustering by the following steps:

1. Determine the proportion of each TS class based upon all TS classes found within a block. These class proportions are useful as they provide a quantitative description of the mineralogical blend characteristics.
2. Average the elemental concentrations to get a unique geochemical signature per block. Since XRF data are compositional in nature, they require a further transformation to log-ratio coordinates to account for closure (Aitchison, 1999). Therefore, the concentrations are transformed by using a centred log-ratio (clr).
3. Combine the TS and XRF features and normalise by a z-score transformation to obtain values in a similar range.
4. Reduce the feature dimension of these block features using PCA. The number of PCs is automatically set to the amount that can describe 95% of the data variance.
5. Cluster the PC dataset using agglomerative hierarchical clustering.

RESULTS/DISCUSSION

Clustering

Clustering of TS data resulted in seven classes using the hull normalised spectra of four wavelength regions. TS Class 2 and 5 discriminated waste rock and are indicated by a dominant FeOH or MgOH-

Ca absorption feature (>2300 nm) showing the mafic nature compared to the felsic rock-related mineralisation. The other classes (1, 3, 4, 6 and 7) show distinct mineralogical patterns related to the gold-bearing material, and accompanying dilution. The white mica composition, the wavelengths at minimum absorption are between 2180 – 2228 nm (W_AlOH), and end-member phengite had significant importance in generating classes. Phengite at TGM is spatially closely associated with gold and shear zones controlling lode geometry (Roache, 2019). The spectra of Class 3 and 4 contain larger proportions of biotite or perhaps amphibole. Class 1, 6 and 7 predominantly discriminate from each other in the following characteristics. Class 6 has a distinct earlier (~605 nm) absorption compared to Class 1 and 7 (~690 nm) in the 500-750 nm region. This Class 6 feature is also shared by Class 4 and relates to increased proportions of epidote. This is also interesting with regards to the material hardness, as will be discussed in the VNIR/SWIR Section. TS Class 7 differentiates from class 1 by a more distinct FeOH absorption shoulder of chlorite around 2250 nm. TS Class 1 contains about 34.8% of all samples of which 40% are above cut-off grade (0.3 ppm Au). The classes will be explained where necessary in the next sections. However, the focus of this paper is on the constitutive proportional relationship of classes with material hardness characteristics.

After the preparation of block features, only blocks with more than ten TS and XRF samples were selected. On average there were 29.5 TS samples and 31.7 XRF samples per block, and there were 4223 blocks in total. Prior to clustering, the seven TS class block proportions and fifteen XRF elemental concentrations (clr transformed) were transformed into thirteen PCs. Clustering of these PCs resulted in seven material types. Figure 4 shows a t-distributed Stochastic Neighbour Embedding (t-SNE) of these PCs into two dimensions (van der Maaten and Hinton, 2011). Each 20x20x20 m block is represented by a scatter point and is coloured by various attributes, such as the material type (class), PC values, Au grade (ppm) and the average elemental concentration and TS class distribution. Note that the Au concentration was not one of the clustering variables. The t-SNE projection shows the relation between the PCs and elements but also links the variables with the clustering classes. It can be seen that material types 1, 5 and 6 are the dominant ore material types, and are characterised by elevated Au, K, S, Si, Nb, Rb, Sr and Zr concentrations (see Figure 4). This is in accordance with previous descriptions of the ore mineralisation (Crawford and Doyle, 2016). The ore also generally has higher proportions of TS Class 1, 6 and 7, whereas the waste material has typically increased TS Class 2 proportions. Material type 5 also has elevated TS Class 4 proportions (43%) and may relate to gold-rich epidote-biotite ore.

Figure 5 shows a three-dimensional representation of the Tropicana pit, and the spatial configuration of the material types represented as blocks. Within the hanging wall, material types 0, 2 and 4 alternate with each other (looking from left to right, Figure 5a and strike E to SE. This indicates that the material types reflect different alteration patterns around shear zones. Material type 0 predominantly occurs in the NE side pit (Figure 5a). Material type 1 correlates with the main ore zone and is sparsely interrupted by material type 6. Material type 5 is predominantly found closer to the footwall (below 1) of the open pit.

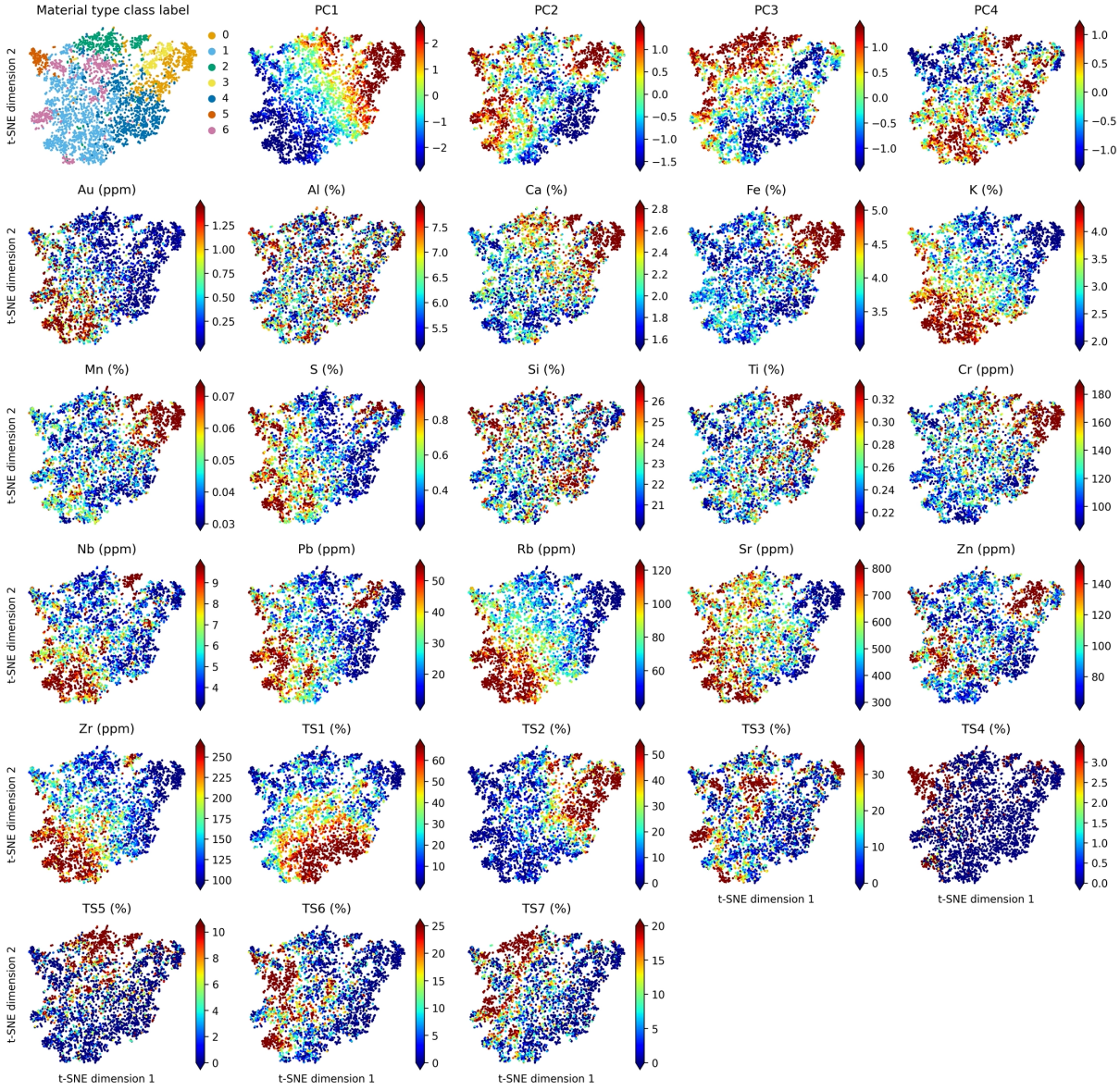

Figure 4. t-Distributed stochastic neighbour embedding projection of 13 principal components into two dimensions for 4233 blocks. Each plot displays one block feature and its corresponding value.

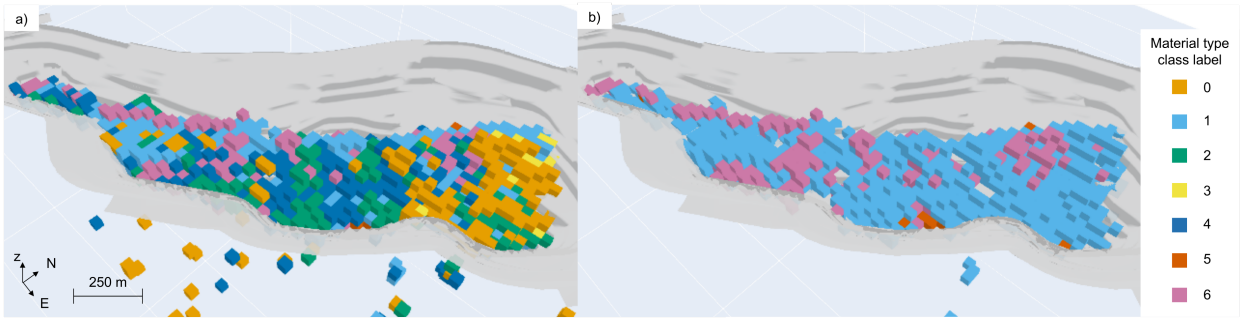

Figure 5. Oblique view of the Tropicana pit displaying the pit outline in light grey; a) blocks (20x20x20m) coloured by material type class labels; b) shows only material type 1, 5 and 6 representing the main ore zone.

Hardness Proxy Relationships

The spatial representation of material types is associated with different ore body hardness domains and thus different distributions of BWi. Metallurgical test results suggest that some preliminary BWi estimates can be made. For example, Table 1 shows that material type 1 is frequently tested, and has an average BWi of 18.33 kWh/t, and Leeb hardness value of 765. These summary statistics suggest that there are hardness variations within material types that can be further subdivided (e.g., a Leeb value between 759-799 may relate with a BWi between 18.54 and 20.72 kWh/t). Projection of relatively sparse metallurgical test data over a whole block is a commonly accepted methodology (e.g., King and Macdonald, 2016; Montoya *et al.,* 2011), but is prone to estimation errors, and is only valid for some mining blocks. A preferred approach is to obtain a material hardness estimate by determining a relationship between the Leeb hardness (Equotip) and BWi per material type. The more frequently (rapid and low cost) collected Equotip rebound hardness measurements can then be used to estimate the BWi and to construct a hardness model.

Table 1. Bond work index and Leeb hardness statistics per material type

Material	BWi (kWh/t)				Equotip (Leeb)			
type	No.[1]	Mean	Std.	IQR[2]	No.[1]	Mean	Std.	IQR[2]
0	4	18.54	0.78	18.0 - 18.4 - 19.0	122	759	91	709 - 782 - 827
1	49	18.33	2.12	16.4 - 18.1 - 20.0	78	765	78	722 - 781 - 818
2	4	18.99	2.64	18.1 - 19.5 - 20.4	30	771	91	734 - 800 - 833
3	3	16.87	1.33	16.1 - 16.2 - 17.3	85	732	101	669 - 743 - 812
4	7	18.10	2.05	17.1 - 18.0 - 18.8	222	767	78	725 - 779 - 823
5	3	19.92	1.60	19.4 - 20.6 - 20.8	6	799	78	772 - 812 - 843
6	11	20.72	1.28	20.3 - 20.9 - 21.5	27	799	75	748 - 793 - 830

[1] Number of blocks, [2] Interquartile range (IQR) displays the 25th, 50th (median) and 75th percentile.

Figure 6 shows the relationship between Leeb hardness and BWi data collected from various studies (Cloete, 2020; Lipton, 2018). This figure includes 42 metallurgical composite samples taken across the TGM deposits. Each TGM point represents a diamond core composite (≤ 5m) analysed for BWi and Equotip rebound hardness (every 10 cm). All Equotip measurements conducted on the composite were averaged. Only composites that conformed to these constraints were considered.

A few observations are made based upon the Equotip-based Leeb hardness versus BWi data in Figure 6:

- The Bowdens Silver project (Lipton, 2018) and Siguiri gold mine data (Cloete, 2020) have representative samples over a range of different hardnesses. They show that there is an existing trend between Leeb hardness and BWi.
- The TGM composite data does not show a definitive relationship between Leeb and BWi. It shows that the ore has a hardness in a smaller Leeb range (640-820) compared to the Bowdens and Siguiri data. The group of TGM samples with a BWi around 15 – 17 kWh/t demonstrates the difficulty in estimating the BWi based upon Leeb. A Leeb of 700 may relate to a work index of 16 kWh/t or 22 kWh/t. This is because TGM composites represent a single rock type; K-feldspar dominated quartzofeldspathic gneiss, and it is thus expected to find the Leeb and BWi in a narrow range. Hunt and Berry, (2017) showed a similar conclusion from data across multiple deposit styles (Archean Au, porphyry Cu and iron oxide copper-gold ore). Sandstone and limestone are also on different hardness trajectories (Park and Kim, 2020).
- Material of significantly different hardnesses gives rise to correlation lines. These correlation lines are specific to locality and an individual area. TGM data may not have captured the variability within the main ore zone or the nature of the composites (blended) smooths the effect of variability.

This material type correlation hypothesis was tested by categorising every TGM composite based upon the material types from the clustering exercise. Unfortunately, this does not show a significant improvement. This may seem strange because every material type has similar and distinct geochemical

and mineralogical properties. However, clear explanations may be found in, for example, the texture and fabric. This may also lead to potential variations in results dependent on whether a destructive (BWi) vs non-destructive (Equotip) test is carried out.

These results show that extrapolating geochemical and mineralogical features for a deterministic material hardness is valid for specific case studies; it requires a significant difference in material hardness. Despite this, the VNIR-SWIR data can still be used to obtain a proxy for the texture through the relative proportion of minerals, and in some cases the crystallinity (Ausspec, 2008). This may be one step closer to understanding the resulting material hardness, however, it does not capture the intergrowth of the constituent minerals and the rock texture. For this reason, it is again necessary to observe the sample within a larger space, i.e., in a theoretical mining block.

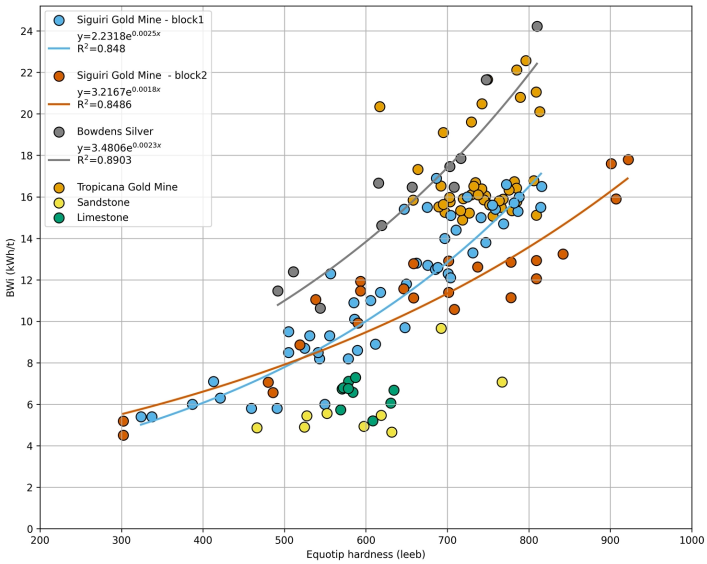

Figure 6. Equotip hardness versus Bond Ball Work Index correlation for various datasets. Sources: Siguiri Gold Mine (Cloete, 2020), Bowdens Silver (Lipton, 2018), sandstone and limestone (Park and Kim, 2020).

VNIR-SWIR

Specific VNIR-SWIR absorption features or regions can provide more information about the relative abundance and nature of mineral intergrowths related to mineral proportions and texture related hardness indications. For example, the relative proportion of white mica (W_AlOH, wavelength of AlOH absorption in 2180-2228 nm) could indicate a sericitic shear zone and thus provide more textural information about the samples, and the relation between Leeb hardness and BWi.

A good location to look for textural differences and their relationship with mineralogical composition is within the Tropicana pit. Figure 7a shows an oblique three-dimensional representation of the Tropicana pit with some of the major shear zones crosscutting the deposit in E to SE direction (Blenkinsop and Doyle, 2014). The blocks are 20x20x20 m and are coloured by the BWi (kWh/t) corresponding to a metallurgical composite found within the block. Note that the same 5 m composite size limit referenced above has not been applied here. The northern end of the pit is marked by a large shear zone obliquely intersecting the line of mineralisation. This shear zone separates a zone of relatively less competent, finer-grained material in the northeast (NE) from a coarse-grained K-feldspathic gneiss in the southwest (SW). This textural change has an impact on the metallurgical test results. BWi results validate this observation (Figure 7a). For example, there is softer material (~15-18 kWh/t) in the northern (NE) end compared to the harder material (>20 kWh/t) in the south (SW). Another set of relatively softer blocks is found near the faults in the middle of Figure 7a. Nevertheless, a detailed mineralogical, geochemical and textural analysis of these rocks still needs to be carried out to confirm the compositional change of these various hardness domains. A potential relationship may be originated from the feldspar-to-mica reactions occurring in these fault zones. During these processes, the released silica may have precipitated in these dilatant sites, increased the

rock strength by cement hardening, and reduced permeability (the SW side). Whereas on the NE side, the transition of feldspars into phengitic (schist-like) micas may have been the dominant strength-controlling (softening) mechanism (Wibberley, 1999).

Figure 7b shows GC samples (≥ 0.5 ppm Au) corresponding with blocks from material type 1 (Figure 5b) as this is the most prominent material type that is found. These samples are geochemically and mineralogically distinct from the other material types, and the following observations are within-class variations, which illustrate the underlying challenges on the projection of one hardness signature over a material type. It should be noted that one can always subdivide material types. However, the spatial and volumetric representativity of each new class may significantly decrease. Figure 7b shows that the shear features can be mapped by a larger relative proportion of phengite (W_ALOH features >2216nm) in the SWIR data. Texturally this rock shows more schistosity, and is an indication for a mica schist-dominated ore type (Roache, 2018). In this context, the schist would be softer (milling) since there are more platy micas and structurally strained/sheared textures. The only problem is that the overall ore signature is also relatively phengitic (across all material types and deposits), and a mica schist character would plot, therefore, close to the mineralised zone spectra for white mica. Additionally, there are no major geochemical differences in a competent sample vs a sample showing progressive foliation.

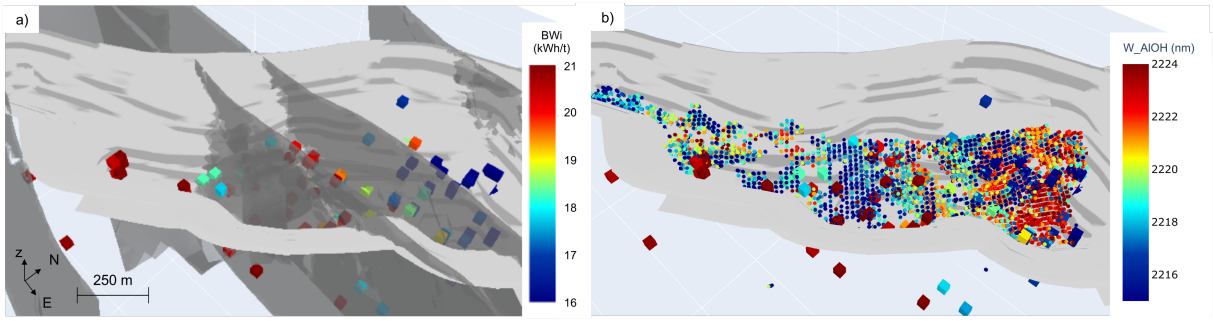

Figure 7. Oblique view of the Tropicana pit displaying the pit outline in light grey; a) major shear zones striking E to SE (dark grey) and blocks (20x20x20m) coloured by BWi (kWh/t) corresponding with a metallurgical composite found within; b) material type 1 (≥ 0.5 ppm Au) GC samples coloured by W_AlOH.

A white mica feature is thus useful for indicating an alteration pattern around shear zones, as demonstrated by various studies. However, the white mica is also an indication of shear planes and thus a potential change in material hardness. In this context, the relationship between white mica and texture is quite restricted. There is the necessity to understand geological structures to implement, for example, a white mica-schist texture proxy. Further analysis of the small geochemical and mineralogical differences between the Tropicana NE and SW zone shows that increasing the number of material classes separates these domains. The source of this separation is established in features represented by principal component 6. This PC is only accountable for 5.2% of the feature variation across the samples. Therefore, this directly provides evidence that the hardness and texture of material are not easily observed by geochemical and mineralogical features, and therefore are not dominant in material type clustering.

Reassessing the main ore material classes and features showed a remarkable match between the normalised hull-quotient spectra in the 600 - 700 nm region and hardness domains. This was already noticed in TS Class 6 (and 4), and is related to a higher portion of TS Class 6 in the softer material (NE). This match may therefore be useful to domain orebody hardnesses and predict the work index. There are also small variations in the average Nb, Ca, and Zn concentration, however, these are not the explanation for the hardness variations. The corresponding samples (material type 1) above ≥ 0.5 ppm Au separated by the NE and SW domain show a significant difference in absorption features.

Figure 8 shows the average hull-quotient corrected spectra from the Tropicana NE and SW domain and the other samples outside the Tropicana pit. The average reflectance spectrum of Tropicana NE has its

minimum absorption close to 600 nm, whereas the reflectance of Tropicana SE, and all other samples outside Tropicana show a more distinct minimum absorption around 690 nm. Commonly, this VNIR region is indicative of iron-bearing minerals (ferric iron (Fe^{3+}) absorption of hematite and goethite) or hydroxylated silicates with Fe, such as chlorite, biotite, epidote (Ausspec, 2008). Figure 8 shows that this feature matches quite well with the hull normalised spectra of epidote in this region (Kokaly *et al.*, 2017). The minimum absorption wavelength of epidote is around 618 nm, but within Tropicana NE, this feature may have shifted slightly due to spectral mixing. This is an indication of an epidote-phengite dominant ore type, which has a significant correlation with softer material (low BWi). This epidote-phengite material is different from material type 5 because material type 1 has significant foliation resulting in a softer work index.

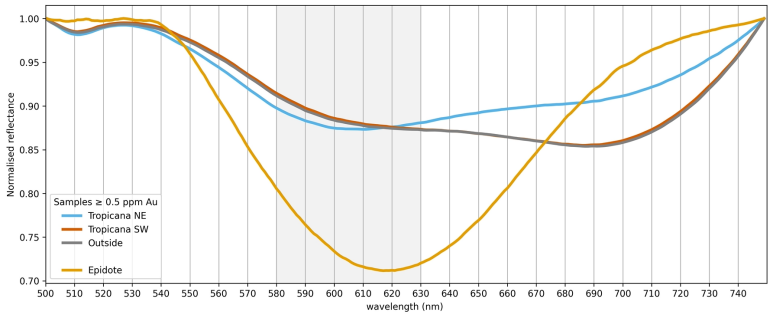

Figure 8. Average hull normalised spectra from material type 1 (≥ 0.5 ppm Au) separated on orebody domain, Tropicana NE, Tropicana SW and outside Tropicana pit. The spectrum of epidote (Kokaly et al., 2017) is provided as a reference for the identified 605 ± 25 nm feature within Tropicana NE.

The W_605 feature of material type 1 GC samples is visualised in Figure 9 and coloured by the minimum absorption wavelength between 580 and 630 nm. This range is chosen because it captures the minimum absorption wavelength for the Tropicana NE ore around 605 nm ± 25 nm (W_605 feature). A low W_605 value indicates that there is a minimum within this zone, and thus that the remaining hull-quotient spectrum increases, whereas a higher value (> 625 nm) indicates that the minimum absorption will be at a higher wavelength (typically around 690 nm). Within material type 1, a high W_605 value corresponds with significantly harder ore and vice versa.

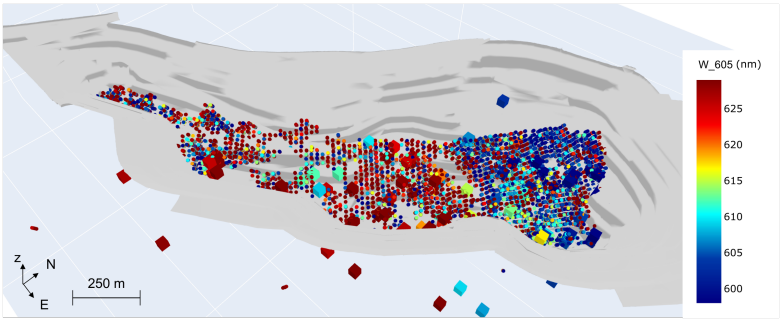

Figure 9. Oblique view of the Tropicana pit displaying the pit outline in light grey and GC samples of material type 1 (≥ 0.5 ppm Au) coloured by W_605 nm. Blocks are coloured by BWi (kWh/t), as in Figure 7a.

CONCLUSION

Material fingerprinting at Tropicana Gold Mine has demonstrated a link between geochemistry, mineralogy and hardness (Leeb, BWi) of various material types. These fingerprints are proxies for the constitutive material hardness properties, and may provide a more comprehensive understanding of comminution behaviour. Each fingerprint was constructed by clustering XRF data, and spectral class proportion of samples found within a small block. The spectral data were represented by four VNIR/SWIR wavelength regions instead of the commonly used individual spectral features. These

smaller region spectra were clustered in classes, and subsequently, class proportions were determined for each block. Clustering of the geochemical and mineralogical data with this approach resulted in an enhanced ore and waste material classification. It is expected that one would be able to readily detect these fingerprints downstream, and infer material characteristics (i.e., for ore/waste separation and material tracking).

Furthermore, predicting the BWi from Equotip rebound hardness is most applicable if a significant variation in material hardness exists. Unfortunately, ore characteristics of TGM fall within a narrow range (16-21 kWh/t) and thus prediction of the work index based upon Equotip measurements may not be definitive. However, the different material types showed that, for example, a better proxy for the work index could be found within the Tropicana NE and SW domain. Within one material type, it was evident that the BWi matched with the newly recognised significance of the W_605 nm region. This indicates the usefulness of the visible wavelength region. This feature could separate one material into a softer (~15-18 kWh/t) and harder (>20 kWh/t) material component. These results may be used for further domaining orebody hardness, and could enhance some of the earlier work index predictions. This outcome has a significant implication for preparing material blends for processing, as well as optimised metallurgical sampling and compositing. Future work may focus on including penetration data as a routinely collected hardness proxy for inclusion in fingerprints. Material texture also plays a major role in the constitutive material hardness, and work is underway to also add a texture proxy to the material fingerprints, as it is hoped that this may improve future work index predictions.

ACKNOWLEDGEMENTS

The authors are grateful to AngloGold Ashanti Ltd. for permission to publish the outputs of the research. Tony Roache and Stephen Brown are thanked for their helpful input, which improved the paper. Ian Lipton and SilverMines Ltd. are thanked for republishing their data.

REFERENCES

Aitchison, J. (1999). *Mathematical Geology*, 31, 563-580.

Ausspec. (2008). *G-MEX Spectral Interpretation Field Manual*, 3rd edn. AusSpec International ltd.

Blenkinsop, T G. and Doyle, M.G. (2014). Structural controls on gold mineralization on the margin of the Yilgarn craton, Albany–Fraser orogen: The Tropicana deposit, Western Australia, *Journal of Structural Geology*, 67, 189-204.

Catto B. (2015). Tropicana Geometallurgy Programme – Integrated Planning. *Internal Report*. AngloGold Ashanti Australia, Tropicana Operation.

Cloete, L.M. (2021). Block 2 Pre-Feasibility Study. *Internal Report*. AngloGold Ashanti, Siguiri Operation.

Crawford, A.J., and Doyle, M.G. (2016). Granulite-Hosted Gold: Tectonic Setting and Lithogeochemistry of the Tropicana Deposit, Western Australia, *Economic Geology*, 111, 395-420.

Dominy, S.C., O'Connor, L., Parbhakar-Fox, A., Glass, H. and Purevgerel, S. (2018). Geometallurgy—A Route to More Resilient Mine Operations. *Minerals*, 8, 560.

Hunt, J.A., and Berry, R.F. (2017). Geological Contributions to Geometallurgy: A Review, *Geoscience Canada*, 44, 103-18.

King, G.S. and Macdonald, J.L. (2016). The business case for early-stage implementation of geometallurgy—An example from the Productora Cu-Au-Mo deposit, Chile. *Proceedings of the International Geometallurgy Conference, Perth, Australia, 15–16 June 2016*. Australasian Institute of Mining and Metallurgy: Melbourne, Australia. pp. 125–133.

Kokaly, R.F., Clark, R.N., Swayze, G.A., Livo, K.E., Hoefen, T.M., Pearson, N.C., Wise, R.A., Benzel, W.M., Lowers, H.A., Driscoll, R.L., and Klein, A.J. (2017). *USGS Spectral Library Version 7: U.S. Geological Survey Data Series 1035*, 61 p.

Lipton, I. (2018). Predicting comminution response using Equotip. *MINEX Conference, Moscow, Russia, 2-4 October 2018*.

Montoya, P., Keeney, L., Jahoda, R., Hunt, J., Berry, R., Drews, U., Chamberlain, V. and Leichliter, S. (2011). Geometallurgical modelling techniques applicable to pre-feasibility projects—La Colosa case study. *Proceedings of the International Geometallurgy Conference, Brisbane, Australia, 5–7 September 2011*. Australasian Institute of Mining and Metallurgy: Melbourne, Australia. pp. 103–111.

Roache, T.J. (2018). Boston Shaker Underground Pre-Feasibility: Geometallurgical domaining. Unedited contribution to the Boston Shaker Underground Pre- Feasibility Study Report. *Internal Report*. AngloGold Ashanti Australia, Tropicana Operation. 9pp.

Roache, T.J. (2019). aiSIRIS mineral interpretation assessment. *Internal Report*. AngloGold Ashanti Australia, Tropicana Operation. 13pp.

Spaggiari, C.V., Kirkland, C.L., Pawley, M.J., Smithies, R.H., Wingate, M.T.D., Doyle, M.G., Blenkinsop, T.G., Clarke, C., Oorschot, L.J., Fox, L.J. and Savage, J. (2011). *The Geology of the East Albany-Fraser Orogene a Field Guide*, Geological Survey of Western Australia, Record 2011/23. p. 98.

Van der Maaten, L. and Hinton, G. (2011). Visualizing non-metric similarities in multiple maps. *Machine Learning*, 87, 33-55.

Van Duijvenbode, J.R., Buxton, M.W.N. and Soleymani Shishvan, M. (2020). Performance Improvements during Mineral Processing Using Material Fingerprints Derived from Machine Learning—A Conceptual Framework. *Minerals*, 10, 366.

Van Duijvenbode, J.R., Cloete, L.M., Soleymani Shishvan, M. S. and Buxton, M.W.N. (in press). A New Approach to Predict Comminution and Recovery Parameters Using Multi-Element Geochemical Data Clustering.

Wambeke, T., Elder, D., Miller, A., Benndorf, J., and Peattie, R. (2018). Real- time reconciliation of a geometallurgical model based on ball mill performance measurements – a pilot study at the Tropicana gold mine. *Mining Technology*, 127 (3), 115-130.

Wibberley, C. (1999). Are feldspar-to-mica reactions necessarily reaction-softening processes in fault zones?, *Journal of Structural Geology*, 21, 1219-27.

Wierzchoń, S.T. and Klopotek, M.A. (2018). Modern Algorithms of Cluster Analysis, Springer.

Jeroen van Duijvenbode

PhD candidate
Delft University of Technology

Jeroen van Duijvenbode is a PhD candidate at Delft University of Technology and performs research on material fingerprinting and understanding how differences in geology influence metallurgical plant performance. The research topic integrates collected information on metallurgical properties directly or through proxies back into the resource model. In his work, he uses sensor data to characterize and classify material for defining diagnostic ore fingerprints. These fingerprints can be tracked through the mining value chain and get better insight in, for example, the energy consumption of the ball mill or recovery process.